Four-Component Scattering Model for Polarimetric SAR Image Decomposition

Yoshio Yamaguchi, *Fellow, IEEE*, Toshifumi Moriyama, *Member, IEEE*, Motoi Ishido, and
Hiroyoshi Yamada, *Member, IEEE*

Abstract—A four-component scattering model is proposed to decompose polarimetric synthetic aperture radar (SAR) images. The covariance matrix approach is used to deal with the non-reflection symmetric scattering case. This scheme includes and extends the three-component decomposition method introduced by Freeman and Durden dealing with the reflection symmetry condition that the co-pol and the cross-pol correlations are close to zero. Helix scattering power is added as the fourth component to the three-component scattering model which describes surface, double bounce, and volume scattering. This helix scattering term is added to take account of the co-pol and the cross-pol correlations which generally appear in complex urban area scatttering and disappear for a natural distributed scatterer. This term is relevant for describing man-made targets in urban area scattering. In addition, asymmetric volume scattering covariance matrices are introduced in dependence of the relative backscattering magnitude between HH and VV. A modification of probability density function for a cloud of dipole scatterers yields asymmetric covariance matrices. An appropriate choice among the symmetric or asymmetric volume scattering covariance matrices allows us to make a best fit to the measured data. A four-component decomposition algorithm is developed to deal with a general scattering case. The result of this decomposition is demonstrated with L-band Pi-SAR images taken over the city of Niigata, Japan.

Index Terms—Polarimetric synthetic aperture radar (POLSAR), radar polarimetry, scattering contribution decomposition, symmetric and asymmetric covariance matrix.

I. INTRODUCTION

TERRAIN and land use classification is one of the most important applications of polarimetric synthetic aperture radar (POLSAR) image data takes. Excellent methods have been proposed to classify terrain based on polarimetric statistical characteristics [1]–[6]. There are two major approaches for a 3×3 polarimetric matrix decomposition. One is the lexicographic covariance matrix approach based on physically measurable parameters [1], and the other is the coherency (Pauli-based covariance) matrix based on mathematically orthogonal Pauli matrix components [3]. Both matrices can be transformed into one another. An overview on decomposition theorem is given in [3].
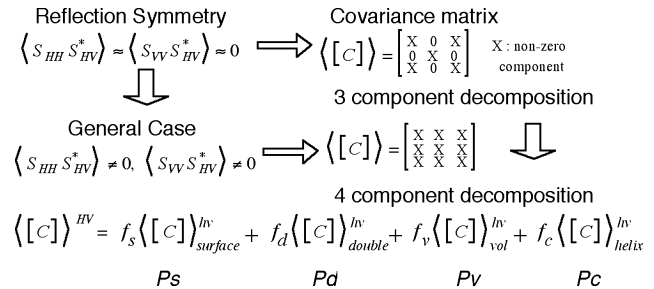
Fig. 1. Four-component scattering model for nonreflection symmetry condition. P_s: surface scattering power. P_d: double-bounce scattering power. P_v: volume scattering power. P_c: helix scattering power.

Three-component scattering power model [1] by Freeman and Durden has been successfully applied to decompose POLSAR image under the well-known reflection symmetry condition $\langle S_{\mathrm{HH}} S_{\mathrm{HV}}^* \rangle \approx \langle S_{\mathrm{VV}} S_{\mathrm{HV}}^* \rangle \approx 0$ using the covariance matrix. This method is based on simple physical scattering mechanisms (surface scattering, double-bounce scattering, and volume scattering), and is powerful for POLSAR image decomposition for natural distributed target areas in the P-L-C band. The advantage of this scattering model is its simplicity and easy implementation for image processing [1], [4], [5].

However, for POLSAR image analysis including urban area scattering for which the reflection symmetry condition does not hold, it is necessary to take the effect of $\langle S_{\mathrm{HH}} S_{\mathrm{HV}}^* \rangle \neq 0$ and $\langle S_{\mathrm{VV}} S_{\mathrm{HV}}^* \rangle \neq 0$ into account. This condition is the nonreflection symmetry constraint, with which most of the research studies have not been dealing with. If we examine covariance matrices in urban areas, we regularly encounter that $\langle S_{\mathrm{HH}} S_{\mathrm{HV}}^* \rangle \neq 0$ and $\langle S_{\mathrm{VV}} S_{\mathrm{HV}}^* \rangle \neq 0$, and the cross-pol component $\langle |S_{\mathrm{HV}}|^2 \rangle$ is rather predominant. The term $\langle |S_{\mathrm{HV}}|^2 \rangle$ contributes only to the volume scattering in the three-component scattering model. These considerations applicable to the reflection-symmetry case are inconsistent with the observed actual scattering phenomena. In order to accommodate the decomposition scheme for the more general scattering case encountered in urban areas or by more complicated geometric scattering structures, it is necessary to introduce another term into the model which corresponds to $\langle S_{\mathrm{HH}} S_{\mathrm{HV}}^* \rangle \neq 0$ and $\langle S_{\mathrm{VV}} S_{\mathrm{HV}}^* \rangle \neq 0$ in the covariance matrix approach of Freeman and Durden [1].

As shown in Fig. 1, we propose to include the helix scattering power as the fourth component for the more general scattering mechanism. This helix scattering power term corresponds to $\langle S_{\mathrm{HH}} S_{\mathrm{HV}}^* \rangle \neq 0$ and $\langle S_{\mathrm{VV}} S_{\mathrm{HV}}^* \rangle \neq 0$, which appears in an urban area whereas disappears for almost all natural distributed scattering. This term is essentially caused by the scattering matrix of helices (or equivalently, left or right circular polarization states)

and is relevant for the complicated shapes of man-made structures, which are predominant in urban areas.

The second point of this paper is a modification of the volume scattering matrix in the decomposition according to the relative backscattering magnitudes of $\langle | S_{HH} |^2 \rangle$ versus $\langle | S_{VV} |^2 \rangle$. In the theoretical modeling of volume scattering, a cloud of a randomly oriented dipole is implemented with a probability function being uniform for the orientation angles [1]. However, for vegetated areas, scattering from tree trunks and branches seems to display a certain characteristic angle distribution. A modification in the orientation angle distribution is proposed for this formulation. This modification yields asymmetric matrices which can be adjusted to measurement data with $\langle | S_{HH} |^2 \rangle \neq \langle | S_{VV} |^2 \rangle$.

In Section II, the theoretical expansion for the covariance matrix of the nonsymmetry case will be presented. Scattering power generated by helix is assigned to the fourth component in Section III, and the orientation angle distribution is modified in Section IV. Based on these theoretical analyses, we propose a four-component decomposition model in Section V, and its adaptation to general POLSAR data takes in Section VI. Finally, some examples with discussions are presented in Section VII.

II. COVARIANCE MATRIX EXPANSION

To derive polarimetric scattering characteristics contained in POLSAR image, it is necessary to evaluate the second-order statistics of its scattering matrices. Here, we follow the scheme given by Freeman and Durden [1] and utilize the covariance matrix approach to derive a four-component scattering model mathematically. Although the covariance matrix is not eigen-based as is the coherency matrix [3] in terms of the Pauli eigenvectors, it is directly related to measurable radar parameters and more straightforward to understand physically. The covariance matrix is defined as

$$\langle [C] \rangle^{HV} = \begin{bmatrix} \langle | S_{HH} |^2 \rangle & \sqrt{2}\langle S_{HH}S_{HV}^* \rangle & \langle S_{HH}S_{VV}^* \rangle \\ \sqrt{2}\langle S_{HV}S_{HH}^* \rangle & 2\langle | S_{HV} |^2 \rangle & \sqrt{2}\langle S_{HV}S_{VV}^* \rangle \\ \langle S_{VV}S_{HH}^* \rangle & \sqrt{2}\langle S_{VV}S_{HV}^* \rangle & \langle | S_{VV} |^2 \rangle \end{bmatrix} \quad (1)$$

where $\langle \rangle$ denotes the ensemble average in the data processing, and the superscript * denotes complex conjugation. For mathematical modeling, however, we need to derive the matrix elements and expand the covariance matrix into basis matrices corresponding to volume, surface, double-bounce scattering, and the remaining scattering component.

Let us start with the scattering matrix where, for simplicity, we define a scattering matrix as

$$[S(HV)] = \begin{bmatrix} S_{HH} & S_{HV} \\ S_{VH} & S_{VV} \end{bmatrix} = \begin{bmatrix} a & c \\ c & b \end{bmatrix} \quad (2)$$

assuming that we are dealing with the backscattering case for which $S_{HV} = S_{VH} = c$. However, we do not neglect the cross-component term S_{HV} so that we can deal with general case. The scattering matrix rotated by an angle θ around the radar line of sight becomes

$$[S(hv)] = \begin{bmatrix} S_{hh} & S_{hv} \\ S_{vh} & S_{vv} \end{bmatrix}$$
$$= \begin{bmatrix} \cos\theta & \sin\theta \\ -\sin\theta & \cos\theta \end{bmatrix} \begin{bmatrix} S_{HH} & S_{HV} \\ S_{VH} & S_{VV} \end{bmatrix} \begin{bmatrix} \cos\theta & -\sin\theta \\ \sin\theta & \cos\theta \end{bmatrix} \quad (3)$$

where the capital letters HV refer to the original polarization measurement bases and also to the measurable quantities, and the small letters hv refer to the rotated coordinates and are used in the mathematical formulation. There is a difference in notation between HV and hv. $\langle [C] \rangle^{HV}$ denotes spatial ensemble averaging of the measured data, and $\langle [C] \rangle^{hv}$ corresponds to mathematical averaging defined by the integration expressions introduced in this paper.

The mathematical form of the covariance matrix elements is obtained via integration using a probability density function $p(\theta)$ according to

$$\langle S_{hh}S_{hh}^* \rangle = \int_0^{2\pi} S_{hh}S_{hh}^* p(\theta)d\theta. \quad (4)$$

The resultant terms are derived as follows:

$$\langle | S_{hh} |^2 \rangle = | a |^2 I_1 + | b |^2 I_2 + | c |^2 I_3 + 2\text{Re}(ab^*)I_4$$
$$+ 2\text{Re}(ac^*)I_5 + 2\text{Re}(bc^*)I_6$$
$$\langle | S_{vv} |^2 \rangle = | a |^2 I_2 + | b |^2 I_1 + | c |^2 I_3 + 2\text{Re}(ab^*)I_4$$
$$- 2\text{Re}(ac^*)I_6 - 2\text{Re}(bc^*)I_5$$
$$\langle | S_{hv} |^2 \rangle = \frac{1}{4} | b - a |^2 I_3 + | c |^2 I_7 + \text{Re}\{c^*(b - a)\}I_8$$
$$\langle S_{hh}S_{vv}^* \rangle = (| a |^2 + | b |^2)I_4 - | c |^2 I_3 + ab^* I_1 + a^* b I_2$$
$$+ (b^*c - ac^*)I_5 + (a^*c - bc^*)I_6$$
$$\langle S_{hh}S_{hv}^* \rangle = a\frac{b^* - a^*}{2}I_5 + b\frac{b^* - a^*}{2}I_6 + c\frac{b^* - a^*}{2}I_3 + ac^* I_{10}$$
$$+ bc^* I_9 + | c |^2 I_8$$
$$\langle S_{hv}S_{vv}^* \rangle = a^*\frac{b - a}{2}I_6 + b^*\frac{b - a}{2}I_5 - c^*\frac{b - a}{2}I_3 + ca^* I_9$$
$$+ b^*c I_{10} - | c |^2 I_8 \quad (5)$$

where

$$I_1 = \int_0^{2\pi} \cos^4\theta \, p(\theta)d\theta$$
$$I_2 = \int_0^{2\pi} \sin^4\theta \, p(\theta)d\theta$$
$$I_3 = \int_0^{2\pi} \sin^2 2\theta \, p(\theta)d\theta$$
$$I_4 = \int_0^{2\pi} \sin^2\theta\cos^2\theta \, p(\theta)d\theta$$
$$I_5 = \int_0^{2\pi} \cos^2\theta\sin 2\theta \, p(\theta)d\theta$$
$$I_6 = \int_0^{2\pi} \sin^2\theta\sin 2\theta \, p(\theta)d\theta$$
$$I_7 = \int_0^{2\pi} \cos^2 2\theta \, p(\theta)d\theta$$
$$I_8 = \int_0^{2\pi} \sin 2\theta\cos 2\theta \, p(\theta)d\theta$$
$$I_9 = \int_0^{2\pi} \sin^2\theta\cos 2\theta \, p(\theta)d\theta$$
$$I_{10} = \int_0^{2\pi} \cos^2\theta\cos 2\theta \, p(\theta)d\theta. \quad (6)$$

If the probability density function is assumed to be uniform, $p(\theta) = 1/(2\pi)$, we have

$$\langle |\, S_{\rm hh}\,|^2 \rangle = \langle |\, S_{\rm vv}\,|^2 \rangle$$
$$= \frac{1}{8} |\, a + b\,|^2 + \frac{1}{4}(|\, a\,|^2 + |\, b\,|^2) + \frac{1}{2} |\, c\,|^2 \quad (7a)$$

$$\langle S_{\rm hh} S_{\rm vv}^* \rangle = \langle S_{\rm hh}^* S_{\rm vv} \rangle$$
$$= \frac{1}{8} |\, a + b\,|^2 + \frac{1}{2}{\rm Re}(a^* b) - \frac{1}{2} |\, c\,|^2 \quad (7b)$$

$$\langle |\, S_{\rm hv}\,|^2 \rangle = \frac{1}{8} |\, a - b\,|^2 + \frac{1}{2} |\, c\,|^2 \quad (7c)$$

$$\langle S_{\rm hh} S_{\rm hv}^* \rangle = \langle S_{\rm hv} S_{\rm vv}^* \rangle = +\frac{j}{2}{\rm Im}\{c^*(a - b)\}. \quad (7d)$$

This uniform distribution yields the volume scattering covariance matrix corresponding to randomly oriented dipoles as

$$\langle [C] \rangle_{\rm dipole}^{\rm hv} = \frac{1}{8} \begin{bmatrix} 3 & 0 & 1 \\ 0 & 2 & 0 \\ 1 & 0 & 3 \end{bmatrix} \quad (8)$$

no matter how we choose $[S]_{\rm v\text{-}dipole}^{\rm HV} = \begin{bmatrix} 0 & 0 \\ 0 & 1 \end{bmatrix}$ representing vertical dipole or $[S]_{\rm h\text{-}dipole}^{\rm HV} = \begin{bmatrix} 1 & 0 \\ 0 & 0 \end{bmatrix}$ for horizontal one.

Similarly, we have for a metallic dihedral corner reflector (double-bounce scatterer)

$$\begin{aligned} [S]_{\rm h\text{-}diplane}^{\rm HV} &= \begin{bmatrix} 1 & 0 \\ 0 & -1 \end{bmatrix} \\ [S]_{\rm v\text{-}diplane}^{\rm HV} &= \begin{bmatrix} -1 & 0 \\ 0 & 1 \end{bmatrix} \end{aligned} \Rightarrow \langle [C] \rangle_{\rm double}^{\rm hv} = \frac{1}{4} \begin{bmatrix} 1 & 0 & -1 \\ 0 & 2 & 0 \\ -1 & 0 & 1 \end{bmatrix}. \quad (9)$$

A single-bounce scatterer (plate or sphere) has the form

$$[S]_{plate}^{\rm HV} = \begin{bmatrix} 1 & 0 \\ 0 & 1 \end{bmatrix} \Rightarrow \langle [C] \rangle_{\rm surface}^{\rm hv} = \frac{1}{2} \begin{bmatrix} 1 & 0 & 1 \\ 0 & 0 & 0 \\ 1 & 0 & 1 \end{bmatrix}. \quad (10)$$

Each element of the covariance matrix remains the same even if the individual scattering matrix is different. This is the advantage for using covariance matrix for target decomposition. In addition, the above forms (8)–(10) satisfy the condition $Trace\langle [C] \rangle = 1$, which means that the total power is unity for each scatterer. The total power is defined as $Trace\langle [C] \rangle$ in this paper. The covariance matrices (8)–(10) are the basic elements of three-component decomposition under the reflection symmetry condition $\langle S_{\rm HH} S_{\rm HV}^* \rangle \approx \langle S_{\rm VV} S_{\rm HV}^* \rangle \approx 0$.

III. CIRCULAR POLARIZATION POWER BY HELIX

Now, it is important to note in (7d) that $\langle S_{\rm hh} S_{\rm hv}^* \rangle$ and $\langle S_{\rm hv} S_{\rm vv}^* \rangle$ yield a certain value for $c^*(a - b) \neq 0$. There is no elementary scatterer except for a right or left helix which satisfies $c^*(a - b) \neq 0$. Since the helix target generates circular polarization for all linear polarization incidence, we may regard

the term as a source of circular polarization generation. In fact we have for the right helix

$$[S]_{r\text{-}helix}^{\rm HV} = \frac{1}{2} \begin{bmatrix} 1 & -j \\ -j & -1 \end{bmatrix} \Rightarrow$$
$$\langle [C] \rangle_{r\text{-}helix}^{\rm hv} = \frac{1}{4} \begin{bmatrix} 1 & j\sqrt{2} & -1 \\ -j\sqrt{2} & 2 & j\sqrt{2} \\ -1 & -j\sqrt{2} & 1 \end{bmatrix} \quad (11a)$$

and for the left helix we have

$$[S]_{l\text{-}helix}^{\rm HV} = \frac{1}{2} \begin{bmatrix} 1 & j \\ j & -1 \end{bmatrix} \Rightarrow$$
$$\langle [C] \rangle_{l\text{-}helix}^{\rm hv} = \frac{1}{4} \begin{bmatrix} 1 & -j\sqrt{2} & -1 \\ j\sqrt{2} & 2 & -j\sqrt{2} \\ -1 & j\sqrt{2} & 1 \end{bmatrix}. \quad (11b)$$

Since $\langle S_{\rm hh} S_{\rm hv}^* \rangle = \langle S_{\rm hv} S_{\rm vv}^* \rangle$ is pure imaginary in the mathematical model, we assign this value as the imaginary part of measured data. In order to avoid conflict with $\langle S_{\rm HH} S_{\rm HV}^* \rangle \neq \langle S_{\rm HV} S_{\rm VV}^* \rangle$ in processing the measured data, we take the average of both for data processing

$$\frac{1}{2}{\rm Im}\{c^*(a - b)\} = \frac{1}{2}{\rm Im}\{\langle S_{\rm HH} S_{\rm HV}^* \rangle + \langle S_{\rm HV} S_{\rm VV}^* \rangle\}. \quad (12)$$

If the magnitude of the helix scattering power is f_c, the corresponding magnitude of $\langle S_{\rm hv} S_{\rm vv}^* \rangle$ becomes $f_c/4$ because the trace of (11) is unity. Therefore the power relation becomes

$$\frac{f_c}{4} = \frac{1}{2} |\, {\rm Im}\{\langle S_{\rm HH} S_{\rm HV}^* \rangle + \langle S_{\rm HV} S_{\rm VV}^* \rangle\}\,|. \quad (13)$$

This power term (13) is taken as the fourth component of a more general decomposition. The sense of rotation is determined by the sign of (12) referring to (11), so that for right circular polarization (RHC) we have

$$ {\rm Im}\{\langle S_{\rm HH} S_{\rm HV}^* \rangle + \langle S_{\rm HV} S_{\rm VV}^* \rangle\} > 0 \quad (14a)$$

and for left circular polarization (LHC) we have

$$ {\rm Im}\{\langle S_{\rm HH} S_{\rm HV}^* \rangle + \langle S_{\rm HV} S_{\rm VV}^* \rangle\} < 0. \quad (14b)$$

IV. CHANGE OF PROBABILITY DENSITY FUNCTION

For volume scattering by vegetation, a randomly oriented dipole model is employed in the three-component scattering model. As shown in Fig. 2, the dipole model is slightly modified considering actual tree trunk and branch distribution. Since vertical structure is rather dominant for forests, tree trunks, and branches, we propose the next probability distribution function for vegetations to be

$$p(\theta) = \begin{cases} \frac{1}{2}\sin\theta, & \text{for } 0 < \theta < \pi \\ 0, & \text{for } \pi < \theta < 2\pi \end{cases} \text{ with } \int_0^{2\pi} p(\theta) d\theta = 1 \quad (15)$$
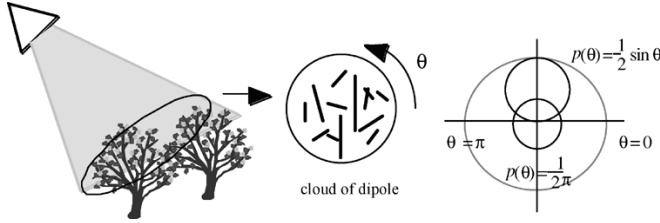
Fig. 2. Probability density distribution function. The angle θ is taken from the horizontal direction seen from the radar line of sight.
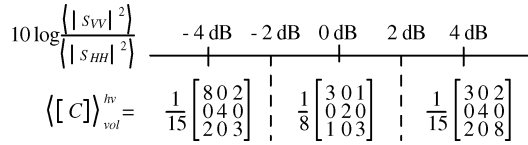

Fig. 3. Choice of the volume scattering covariance matrix $\langle [C] \rangle_{\mathrm{vol}}^{\mathrm{hv}}$ according to the value of $10 \log (\langle | S_{\mathrm{VV}} |^2 \rangle / \langle | S_{\mathrm{HH}} |^2 \rangle)$.

where θ is taken from the horizontal axis seen from the radar. In this case, the integrals (6) lead to

$$I_1 = \frac{3}{15} \qquad I_2 = I_3 = \frac{8}{15} \qquad I_4 = \frac{2}{15}$$

$$I_5 = I_6 = I_8 = 0 \qquad I_9 = -\frac{6}{15} \qquad I_{10} = \frac{1}{15}. \qquad (16)$$

These values (16) result in the volume scattering covariance matrix to become for the vertical dipole

$$[S]_{\text{v-dipole}}^{\mathrm{HV}} = \begin{bmatrix} 0 & 0 \\ 0 & 1 \end{bmatrix} \Rightarrow \langle [C] \rangle_{\mathrm{vol}}^{\mathrm{hv}} = \frac{1}{15} \begin{bmatrix} 8 & 0 & 2 \\ 0 & 4 & 0 \\ 2 & 0 & 3 \end{bmatrix} \quad (17a)$$

and for the horizontal dipole

$$[S]_{\text{h-dipole}}^{\mathrm{HV}} = \begin{bmatrix} 1 & 0 \\ 0 & 0 \end{bmatrix} \Rightarrow \langle [C] \rangle_{\mathrm{vol}}^{\mathrm{hv}} = \frac{1}{15} \begin{bmatrix} 3 & 0 & 2 \\ 0 & 4 & 0 \\ 2 & 0 & 8 \end{bmatrix}. \quad (17b)$$

This asymmetric form (17) seems to be of considerable use because it can be adjusted to the measured data with $\langle | S_{\mathrm{HH}} |^2 \rangle \neq \langle | S_{\mathrm{VV}} |^2 \rangle$. It is known that the HH component is larger than the VV component in forests in the L-band, i.e., 0.2–2.1 dB by AIRSAR measurement data [1], [2], and 1.4 dB for a planted forest area by Pi-SAR measurement data [12], respectively.

Note that the covariance forms (17) remain the same if the distribution function is chosen as $(1/2) \cos \theta$ for horizontal dipole. Since POLSAR data exhibit various relative magnitudes for $\langle | S_{\mathrm{HH}} |^2 \rangle$ and $\langle | S_{\mathrm{VV}} |^2 \rangle$ depending on the scene, we can choose an appropriate covariance matrix set according to the relative measurement value. Since the ratio of $\langle | S_{\mathrm{hh}} |^2 \rangle$ and $\langle | S_{\mathrm{vv}} |^2 \rangle$ in (17) is $10 \log (8/3) = 4.26 \approx 4$ dB, the boundary and regime are set in Fig. 3 for appropriate choices of $\langle [C] \rangle_{\mathrm{vol}}^{\mathrm{hv}}$. If the relative magnitude difference is larger than 2 dB, we choose one of the asymmetric forms (17). If the difference is within ± 2 dB, we choose the symmetric form (8). This adaptation can be applied not only to vegetation areas but also to urban areas. As a result, this choice allows us to make a straightforward best fit to measured data.

V. FOUR-COMPONENT DECOMPOSITION

Double-bounce structure includes road surface—building wall, ground-trees, and man-made targets. Using the Fresnel reflection coefficients, the scattering matrices and the covariance matrices are further modeled in [1] as

$$[S]_{\text{double}} = \begin{bmatrix} \alpha & 0 \\ 0 & 1 \end{bmatrix} \Rightarrow \langle [C] \rangle_{\text{double}}^{\mathrm{hv}} = \begin{bmatrix} |\alpha|^2 & 0 & \alpha \\ 0 & 0 & 0 \\ \alpha^* & 0 & 1 \end{bmatrix}. \quad (18)$$

For surface scattering, the covariance matrix becomes

$$[S]_{\text{surface}} = \begin{bmatrix} \beta & 0 \\ 0 & 1 \end{bmatrix} \Rightarrow \langle [C] \rangle_{\text{surface}}^{\mathrm{hv}} = \begin{bmatrix} |\beta|^2 & 0 & \beta \\ 0 & 0 & 0 \\ \beta^* & 0 & 1 \end{bmatrix} \quad (19)$$

α and β are unknown parameters to be determined later.

Using the four-component approach with (8), (11), (17)–(19), we expand the measured covariance matrix as

$$\begin{aligned}
\langle [C] \rangle^{\mathrm{HV}} &= f_s \langle [C] \rangle_{\text{surface}}^{\mathrm{hv}} + f_d \langle [C] \rangle_{\text{double}}^{\mathrm{hv}} + f_v \langle [C] \rangle_{\text{vol}}^{\mathrm{hv}} \\
&\quad + f_c \langle [C] \rangle_{\text{helix}}^{\mathrm{hv}} \\
&= f_s \begin{bmatrix} |\beta|^2 & 0 & \beta \\ 0 & 0 & 0 \\ \beta^* & 0 & 1 \end{bmatrix} + f_d \begin{bmatrix} |\alpha|^2 & 0 & \alpha \\ 0 & 0 & 0 \\ \alpha^* & 0 & 1 \end{bmatrix} \\
&\quad + \frac{f_v}{15} \begin{bmatrix} 8 & 0 & 2 \\ 0 & 4 & 0 \\ 2 & 0 & 3 \end{bmatrix} + \frac{f_c}{4} \begin{bmatrix} 1 & \pm j\sqrt{2} & -1 \\ \mp j\sqrt{2} & 2 & \pm j\sqrt{2} \\ -1 & \mp j\sqrt{2} & 1 \end{bmatrix}
\end{aligned}$$
$$(20)$$

where f_s, f_d, f_v, and f_c are the expansion coefficients to be determined. The first and the second terms are identical with those in [1]; the third term is modified for data with $10 \log (\langle | S_{\mathrm{HH}} |^2 \rangle / \langle | S_{\mathrm{VV}} |^2 \rangle) > 2$ dB; and the fourth term is introduced for encountering the helix scattering power contribution. Now comparing the covariance matrix elements, we have the following five equations with six unknowns α, β, f_s, f_d, f_v, and f_c:

$$\langle | S_{\mathrm{HH}} |^2 \rangle = f_s |\beta|^2 + f_d |\alpha|^2 + \frac{8}{15} f_v + \frac{f_c}{4} \quad (21a)$$

$$\langle | S_{\mathrm{HV}} |^2 \rangle = \frac{2}{15} f_v + \frac{f_c}{4} \quad (21b)$$

$$\langle | S_{\mathrm{VV}} |^2 \rangle = f_s + f_d + \frac{3}{15} f_v + \frac{f_c}{4} \quad (21c)$$

$$\langle S_{\mathrm{HH}} S_{\mathrm{VV}}^* \rangle = f_s \beta + f_d \alpha + \frac{2}{15} f_v - \frac{f_c}{4} \quad (21d)$$

$$\frac{1}{2} \mathrm{Im}\{ \langle S_{\mathrm{HH}} S_{\mathrm{HV}}^* \rangle + \langle S_{\mathrm{HV}} S_{\mathrm{VV}}^* \rangle \} = \frac{f_c}{4}. \quad (21e)$$

Since the left-hand side of (21) is measurable quantity, we can determine f_c directly with the aid of (13)

$$\begin{aligned}
f_c = P_c &= 2| \mathrm{Im}\{ \langle S_{\mathrm{HH}} S_{\mathrm{HV}}^* \rangle + \langle S_{\mathrm{HV}} S_{\mathrm{VV}}^* \rangle \} | \\
&= 2| \mathrm{Im} \langle S_{\mathrm{HV}}^* (S_{\mathrm{HH}} - S_{\mathrm{VV}}) \rangle |. \quad (22)
\end{aligned}$$

Then, (21b) gives the volume scattering coefficient f_v directly as

$$f_v = \frac{15}{2} \left(\langle | S_{\mathrm{HV}} |^2 \rangle - \frac{f_c}{4} \right). \quad (23)$$

In the left column figure (Fig. 3):

$$10 \log \frac{\langle | S_{VV} |^2 \rangle}{\langle | S_{HH} |^2 \rangle}$$

$$-4\text{ dB} \quad -2\text{ dB} \quad 0\text{ dB} \quad 2\text{ dB} \quad 4\text{ dB}$$

$$\langle [C] \rangle_{vol}^{hv} = \frac{1}{15} \begin{bmatrix} 8 & 0 & 2 \\ 0 & 4 & 0 \\ 2 & 0 & 3 \end{bmatrix} \quad \frac{1}{8} \begin{bmatrix} 3 & 0 & 1 \\ 0 & 2 & 0 \\ 1 & 0 & 3 \end{bmatrix} \quad \frac{1}{15} \begin{bmatrix} 3 & 0 & 2 \\ 0 & 4 & 0 \\ 2 & 0 & 8 \end{bmatrix}$$

It is interesting to note that the numerical coefficient to $\langle | S_{HV} |^2 \rangle$ becomes 7.5 with this expansion (17a), compared to 8 in the uniform expansion (8) for the three-component scattering model [1].

The remaining four unknowns with three equations can be obtained in the same manner as shown in [1]. The scattering powers, P_s, P_d, P_v, and P_c, corresponding to surface, double bounce, volume, and helix contributions, respectively, are obtained as

$$P_s = f_s(1 + | \beta |^2) \qquad P_d = f_d(1 + | \alpha |^2)$$
$$P_v = f_v \qquad\qquad P_c = f_c \tag{24}$$
$$P_t = P_s + P_d + P_v + P_c = \langle | S_{HH} |^2 + 2| S_{HV} |^2 + | S_{VV} |^2 \rangle. \tag{25}$$

The above [(20)–(25)] are the main set of expressions for the four-component decomposition.

VI. ALGORITHM FOR THE FOUR-COMPONENT DECOMPOSITION TO POLSAR DATA

When we apply the four-component decomposition scheme to POLSAR data directly, we sometimes encounter a problem in that the coefficient f_s or f_d becomes negative for certain areas. Since the negative coefficient indicates the corresponding power is negative, it is inconsistent with the physical phenomenon. A typical feature of such areas is that $\langle | S_{HV} |^2 \rangle$ is rather predominant compared to $\langle | S_{HH} |^2 \rangle$ and to $\langle | S_{VV} |^2 \rangle$. These areas reside within small sections of geometrically complicated man-made scattering (cultivated) and of forested areas. In order to avoid such incontinency, we devised an algorithm for the four-component decomposition which could be applied to general POLSAR data image analyses.

The main point to avoid inconsistency is to use the following power ratio:

$$2\langle | S_{HV} |^2 \rangle : \langle | S_{HH} |^2 \rangle \text{ or } \langle | S_{VV} |^2 \rangle \tag{26}$$

based on statistics [7], [8] and on our experiences of POLSAR image analysis [9]. The theoretical studies showed that co-pol radar channel power and cross-pol channel power are of the magnitude ratio of $2:1$ statistically [7], [8]. This condition is used in the middle stage of the four-component decomposition algorithm in Fig. 4.

Fig. 4 shows the algorithm for four-component scattering power decomposition when applied to general POLSAR data. The scheme consists of the following steps.

Step 1) The helix scattering power P_c is directly determined by **(22)** using measured data.
Step 2) The volume scattering power P_v is then determined directly according to the choice of $\langle [C] \rangle_{vol}^{hv}$ and according to the relative magnitude of $\langle | S_{HH} |^2 \rangle$ and $\langle | S_{VV} |^2 \rangle$ as shown in **Fig. 3**. The appropriate choice of $\langle [C] \rangle_{vol}^{hv}$ would make a best-match for volume scattering. If $\langle [C] \rangle_{vol}^{hv}$ is chosen as **(17a)**, the corresponding P_v is given by **(23)**.
Step 3) If $2\langle | S_{HV} |^2 \rangle < \langle | S_{HH} |^2 \rangle$ or $\langle | S_{VV} |^2 \rangle$ holds in the selected area, P_s and P_d can be determined by
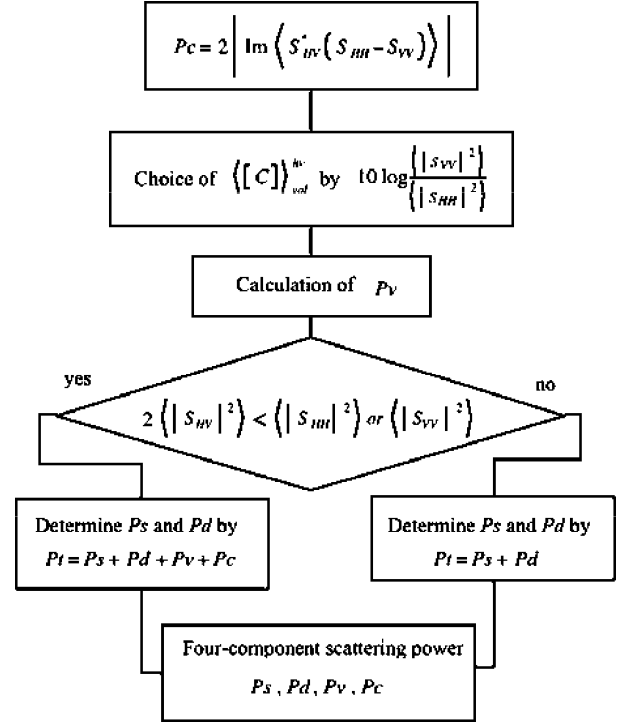

Fig. 4. Algorithm for the four-component scattering power decomposition.

the total power relation **(25)**. This case corresponds to the main scheme of the four-component decomposition proposed in this paper.
If $2\langle | S_{HV} |^2 \rangle > \langle | S_{HH} |^2 \rangle$ or $\langle | S_{VV} |^2 \rangle$ holds in the area, we determine f_s and f_d by the three-component decomposition algorithm **[1]**

$$\langle | S_{HH} |^2 \rangle = f_s| \beta |^2 + f_d| \alpha |^2$$
$$\langle | S_{VV} |^2 \rangle = f_s + f_d$$
$$\langle S_{HH} S_{VV}^* \rangle = f_s\beta + f_d\alpha. \tag{27}$$

The surface scattering power P_s and the double-bounce scattering power P_d can be obtained in the same manner **[1]**.
Step 4) The four-component decomposition is completed, yielding P_s, P_d, P_v, and P_c, even though there is a decision-making step inserted in the algorithm.

Although this four-component decomposition is intended to apply to nonreflection symmetry case, the scheme automatically includes the reflection symmetry condition. The nonreflection symmetry condition is incorporated in the expression of P_c in (22), and in that sense, this method is an extension of three-component decomposition.

VII. EXAMPLE AND DISCUSSION

An L-band Pi-SAR dataset was used for the four-component decomposition. The Pi-SAR sensor is an airborne POLSAR system developed by former Communications Research Laboratory (now NICT) and NASDA (now JAXA) of Japan. The resolution in the L-band image is 3 m $\times$ 3 m. The area chosen
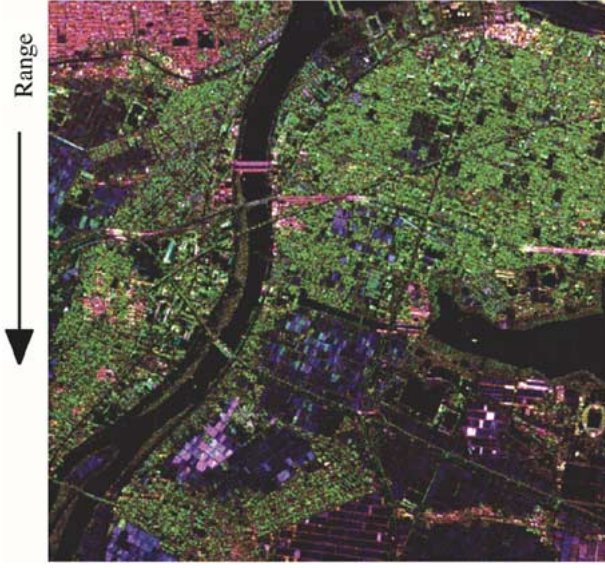
Fig. 5. Color composite polarimetric image of Toyano Ward area in Niigata city: HH (red), VV (blue), HV (green).

for analysis is the Toyano ward in Niigata city, Japan, which includes an urban area, a lake, a river, and paddy rice fields. A color image of polarization decomposition of the scattering matrix is shown in Fig. 5 with HH (red), VV (blue), and HV (green).

Polarimetric calibration [10] is carried out in advance of the decomposition. Polarimetric calibration is important to decompose the helix scattering contribution properly as we can see the corresponding term $\mathrm{Im}\{\langle S_{\mathrm{HH}}S_{\mathrm{HV}}^* \rangle + \langle S_{\mathrm{HV}}S_{\mathrm{VV}}^* \rangle\}$ in (12). This term is directly related to helix scattering power P_c which is then related to the remaining power terms P_v, P_s, and P_d.

The decomposed color image of the covariance matrix with P_s (blue), P_d (red), and P_v (green) is shown in Fig. 6(a). It is seen in Fig. 6(a) that P_d (red) is especially strong in some urban areas (upper left corner and small portion of upper right corner). The red area has a common feature that the orientation of building blocks is parallel to the SAR flight path. The same is true for bridges over a river and some sections along roads indicated by red lines. The pink colored area (lower left corner) in Fig. 5 is decomposed to be a blue one in Fig. 6 indicating P_s is dominant. This blue area corresponds to rice paddy field with the ridge orientation not parallel to flight path. Since there is no other scattering mechanism except for single bounce in the rice field, the decomposition result is acceptable. Most of the upper right quadrant is urban area where the orientation of building blocks is not parallel to the flight path. These areas with skew-oriented building blocks produce a rather predominant HV component. Therefore, the helix scattering component P_c appears strong in these areas as shown in Fig. 6(b). Although the actual source of circular polarization is difficult to explain, it is known theoretically that 45°-oriented four dipoles with spacing of $\lambda/8$ wavelength [11] in the range direction or that 45°-oriented dihedral corner reflector pairs with $\lambda/4$ wavelength range spacing generate a complete circular polarization
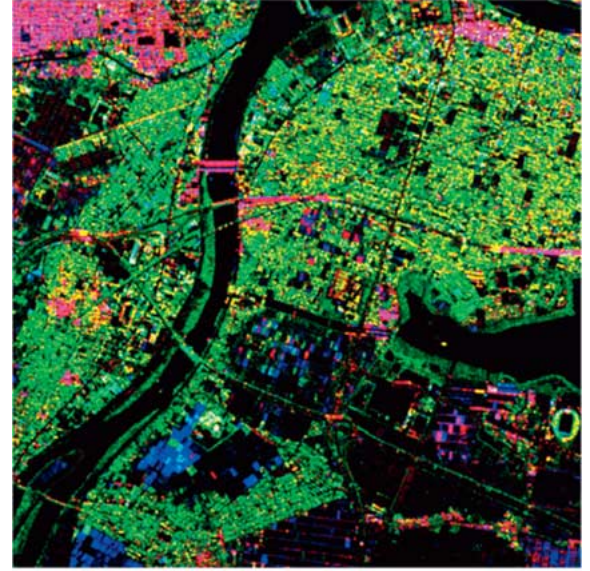
(a)

(b)

Fig. 6. Decomposed image of Fig. 5. (a) The image is colored by P_s (blue), P_d (red), and P_v (green). (b) Helix scattering power P_c.

TABLE I
RELATIVE MAGNITUDE (IN DECIBELS) OF DECOMPOSED POWER NORMALIZED TO SURFACE SCATTERING POWER P_s IN FIG. 6

Max	Ps	Pd	Pv	Pc
(dB)	0	-1.5	-0.45	-3.0

return. It is anticipated that these source structures are present in complicated scattering environments within urban areas. A circularly geomeric shaped structure seen in the right lower corner of Fig. 6(b) is a soccer stadium with a round waving roof. Fig. 6 shows that the entire image decomposition is satisfying electromagnetic vector (polarization) scattering principles.

Table I shows the relative magnitudes of decomposed power terms in Fig. 6. The maximum magnitudes are shown for comparison. The averaged magnitude of P_c is usually down by a factor of 8–10 dB compared to the other components.
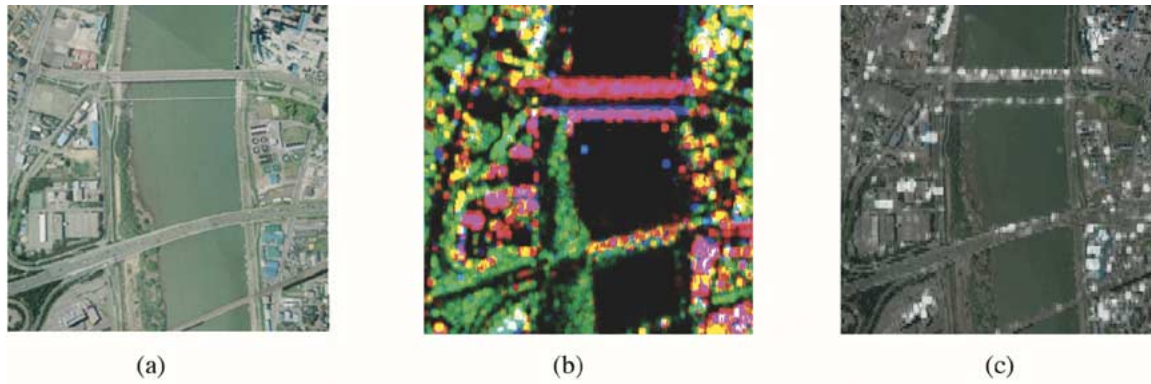
Fig. 7. Zoomed up image around the river. (a) A photo. (b) P_s (blue), P_d (red), and P_v (green), (b) Overlay image of P_c to (a).

TABLE II
FOUR-COMPONENT VERSUS THREE-COMPONENT EXECUTION
RATIO FOR DIFFERENT POLSAR SCENES

	Four-component	Three-component
Toyamo Area of Fig.6	55.5 %	44.5 %
Planted forested area	49.1	50.9
Niigata University area	80.6	19.4

In order to demonstrate the validity of the four-component scattering model more clearly, we zoomed up a small area within Fig. 6 to see the actual correspondence with the contributing scattering structures. Fig. 7 displays the chosen area consisting of: (a) an aerial photo, (b) decomposed image by P_s, P_d, and P_v, (c) overlay image of P_c on (a). The dominant component for the scattering from the bridge over the river is the double-bounce power P_d caused by bridge-water surface reflection. As being anticipated from the electromagnetic vector scattering point of view, we can observe the proper magnitude (red color) distribution resulting from bridges with respect to the radar illumination direction. Buildings near the bridges whose facets are parallel to flight path exhibit strong P_d, whereas buildings with nonparallel orientation to flight path exhibit other strong components in Fig. 7(b). The location of strong P_c can be identified in (c) from the overlay image. From inspection of Fig. 7(c), we can see that strong P_c is generated from facets of man-made targets due to complex multiple scattering effects.

We have applied the four-component decomposition scheme to various radar scenes acquired by Pi-SAR including cultivated and planted forested areas including complicated heterogeneous man-made structures within the vicinity of the Niigata University, Ikarashi Campus. Since the developed algorithm is adjustable to the general scattering case, the decomposition result has been successful when applied to a great many other scenes. Instead of depicting other images, we calculated the ratio of four-component decomposition with respect to the three-component decomposition based on (26). The percentage variation is provided in Table II. Approximately 50% of computer execution went through the main stream of four-component decomposition.

VIII. CONCLUSION

A four-component scattering model based on the covariance matrix is proposed for polarimetric SAR data decomposition.

The four components are identified by single bounce, double bounce, volume, and helix scattering power contributions. The decomposition scheme incorporates the nonreflection symmetry condition, which has not been dealt with previously in the literature. The fourth component, a helix scattering power term, corresponds to the imaginary part of $\langle S_{\mathrm{HH}} S_{\mathrm{HV}}^* \rangle$, which often appears in complex urban areas and disappears in naturally distributed scattering scenarios. On the other hand, the volume scattering component for vegetation is modified by a change of the probability density function for the associated orientation angles. The choice between the symmetric and the asymmetric covariance can be determined by the relative magnitude between $\langle | S_{\mathrm{HH}} |^2 \rangle$ and $\langle | S_{\mathrm{VV}} |^2 \rangle$ of the image data chosen. Hence an algorithm was developed which takes account of the physical randomness. The four-component decomposition scheme result is demonstrated with implementation of L-band Pi-SAR image data takes collected over the Toyano Ward of Niigata city, Japan.

REFERENCES

[1] A. Freeman and S. L. Durden, "A three-component scattering model for polarimetric SAR data," *IEEE Trans. Geosci. Remote Sens.*, vol. 36, no. 3, pp. 963–973, May 1998.
[2] R. Kwok, E. Rignot, J. Way, A. Freeman, and J. Holt, "Polarization signatures of frozen and thawed forest of varying environment state," *IEEE Trans. Geosci. Remote Sens.*, vol. 32, no. 2, pp. 371–381, Mar. 1994.
[3] S. R. Cloude and E. Pottier, "A review of target decomposition theorems in radar polarimetry," *IEEE Trans. Geosci. Remote Sens.*, vol. 34, no. 2, pp. 498–518, Mar. 1996.
[4] J. S. Lee, M. R. Grunes, T. L. Anisworth, L. Du, D. L. Schuler, and S. R. Cloude, "Unsupervised classification using polarimetric decomposition and the complex Whishart classifier," *IEEE Trans. Geosci. Remote Sens.*, vol. 37, no. 5, pp. 2249–2258, Sep. 1999.
[5] J. S. Lee, M. R. Grunes, E. Pottier, and L. F. Famil, "Unsupervised terrain classification preserving polarimetric scattering characteristics," *IEEE Trans. Geosci. Remote Sens.*, vol. 42, no. 4, pp. 722–731, Apr. 2004.
[6] Y. Dong, B. C. Foster, and C. Ticehurst, "A new decomposition of radar polarization signatures," *IEEE Trans. Geosci. Remote Sens.*, vol. 36, no. 3, pp. 933–939, May 1998.
[7] Y. Ke, "Notes on invariant characters of radar cross sections," in *Proc. 2001 CIE Int. Conf. Radar*, 2001, pp. 418–422.

[8] J. Yang, "On Theoretical Problems in Radar Polarimetry," Ph.D, Niigata Univ., Graduate School Sci. Technol., Niigata, Japan, 2000.

[9] Y. Yamaguchi, Y. Takayanagi, W. -M. Boerner, H. J. Eom, and M. Sengoku, "Polarimetric enhancement in radar channel imagery," *IEICE Trans. Commun.*, vol. E78-B, no. 8, pp. 1571–1579, 1995.

[10] J. van Zyl, "Calibration of polarimetric radar images using only image parameters and trihedral corner reflector responses," *IEEE Trans. Geosci. Remote Sens.*, vol. 28, no. 3, pp. 337–348, May 1990.

[11] K. Kitayama, Y. Yamaguchi, J. Yang, and H. Yamada, "Compound scattering matrix of targets aligned in the range direction," *IEICE Trans. Commun.*, vol. E84-B, no. 1, pp. 81–88, 2001.

[12] M. Shimada, "Determination of polarimetric calibration parameters of L band SAR using uniform forest area," presented at the *PI-SAR Workshop*, 2003.

[13] K. Kimura, Y. Yamaguchi, and H. Yamada, "Circular polarization correlation coefficient for detection of nonnatural targets aligned not parallel to SAR flight path in the X-band POLSAR image analysis," *IEICE Trans. Commun.*, vol. E87-B, no. 10, pp. 3050–3056, 2004.

Toshifumi Moriyama (M'98) was born in Fukui Prefecture, Japan, on January 1, 1972. He received the B.E., M.E., and Ph.D. degrees in information engineering from Niigata University, Niigata, Japan, in 1994, 1995, and 1998, respectively.

He was with Fujitsu System Integration Laboratories, Ltd. from 1998 to 2003. He is now with the National Institute of Information and Communications Technology, Tokyo, Japan. His interests are in radar polarimetry and microwave remote sensing.

Dr. Moriyama received the IEEE AP/S Tokyo Chapter Young Engineer Award in 1998 and is a member of IEICE of Japan and the Remote Sensing Society of Japan.

Motoi Ishido graduated from Niigata University, Niigata, Japan, in 2002. He is currently pursuing the M.E. degree in information engineering, where he is engaged in POLSAR image analysis.

Yoshio Yamaguchi (M'83–SM'94–F'02) received the B.E. degree in electronics engineering from Niigata University, Niigata, Japan, and the M.E. and Dr.Eng. degrees from the Tokyo Institute of Technology, Tokyo, Japan, in 1976, 1978, and 1983, respectively.

In 1978, he joined the Faculty of Engineering, Niigata University, where he is a Professor and Head of the Information Engineering Department. From 1988 to 1989, he was a Research Associate at the University of Illinois at Chicago. His interests are in the field of radar polarimetry, microwave sensing, and imaging.

Dr. Yamaguchi has served as Chair of IEEE GRSS Japan Chapter (2002–2003), Vice-Chair (2000–2001), Organizer of PI-SAR Workshops (2000–2005) in Japan, and Associate Editor for Asian affairs of GRSS NEWSLETTER since 2003. He is a member of IEICE of Japan.

Hiroyoshi Yamada (M'93) received the B.E., M.E., and Dr.Eng. degrees from Hokkaido University, Hokkaido, Japan, in 1988, 1990, and 1993, respectively, all in electronic engineering.

In 1993, he joined the Faculty of Engineering, Niigata University, Niigata, Japan, where he is an Associate Professor. From 2000 to 2001, he was a Visiting Scientist at the Jet Propulsion Laboratory, California Institute of Technology, Pasadena. His interests include the fields of array signal processing, polarimetric radar interferometry, and high-resolution techniques.

Dr. Yamada is a member of IEICE of Japan.